Towards an improved spatial representation of a boundary layer from the attached eddy model

Felix Eich [1,*] Charitha M. de Silva [2,†] Ivan Marusic,[3] and Christian J. Kähler[1]

[1]*Institute of Fluid Mechanics and Aerodynamics, Bundeswehr University Munich, 85577 Neubiberg, Germany*
[2]*School of Mechanical and Manufacturing Engineering, University of New South Wales, Sydney 2052, Australia*
[3]*Department of Mechanical Engineering, University of Melbourne, Victoria 3010, Australia*

This study compares the predicted synthetic flow fields generated based on the representative structures of the attached eddy model to experimental data captured using Particle Image Velocimetry of a turbulent boundary layer. To this end, wall-parallel and cross-stream planar fields are analyzed qualitatively and quantitatively by examining instantaneous flow features and by statistical two-point correlation functions, respectively. Our results reveal that although single-point flow statistics are in good agreement with the experimental data, a comparison of instantaneous flow fields and multipoint statistics between the attached eddy model and experiments shows differences in the spatial coherence. Based on these observations, a modification to the placement of the representative eddies in the attached eddy model is proposed that incorporates the meandering of these flow structures, which has been extensively reported in turbulent boundary layers. Our results reveal that this subtle modification provides a superior spatial representation of a turbulent boundary layer from the attached eddy model by reducing periodic effects and the overestimated spatial coherence. Similar improvements are also reported for the spatial representation of the spanwise velocity component.

I. INTRODUCTION

The coherent structures in turbulent boundary layers have been the subject of many investigations, as documented in recent reviews by Jiménez [1] and Wallace [2]. Over the past few decades, coherent structures have become a key focus of research, alongside the statistical and mean flow description of a turbulent boundary layer [3,4]. In his review on coherent structures in turbulent boundary layers, Robinson [5] highlights the importance of coherent flow structures to understand the complex chaotic turbulent motions within boundary layers. Further, through the concept of coherence, the generation, transport, and decay of turbulence itself can be qualitatively understood. To characterize these coherent structures along with their origin and dynamics, analytical models have been theorized. However, because of their inherent complexity, the structural framework of boundary layers is notoriously resistant to attempts at physical modeling.

The most well-known structure-based models of a turbulent boundary layer are the hairpin model [6,7] and the attached eddy model (AEM) [8]. While the hairpin model allows understanding many aspects of the turbulent motions qualitatively [3,9], the AEM, first introduced by Townsend [8] and

---

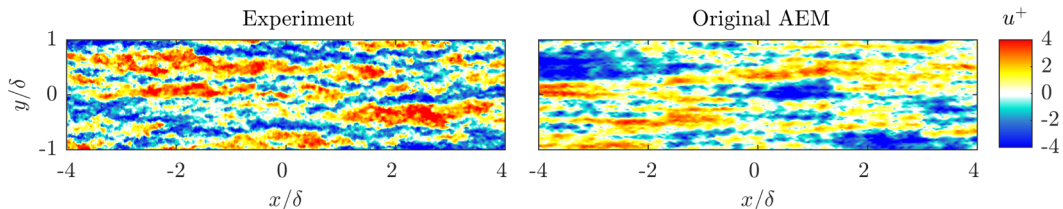*felix.eich@unibw.de
†c.desilva@unsw.edu.au

FIG. 1. Instantaneous streamwise velocity fluctuations u^+ on a wall-parallel plane (xy) at wall-normal height of $z/\delta \approx 0.06$ (within the logarithmic region). Left: Experimental data at $\mathrm{Re}_\tau \approx 4200$. Right: Synthetic flow field generated based on the attached eddy model at $\mathrm{Re}_\tau = 3200$.

later extended by Perry *et al.* [10] and Marusic and Perry [11] has been shown to successfully model the single point statistics of turbulent boundary layers, including higher-order statistics quantitatively [12,13]. The AEM, recently reviewed by Marusic and Monty [14], was originally conceived to represent single point flow statistics in the logarithmic layer based on vortices of archlike structures that are inclined with respect to the wall. The concept of arch- or hairpinlike flow structures were derived from extended flow visualizations at low Reynolds numbers using hydrogen bubbles or smoke [15,16]. These visualizations show the Lagrangian flow properties, while more recently, PIV measurements revealed the existence of these structures through a Eulerian description. Specifically, Adrian *et al.* [9] confirmed the presence of hairpin-type vortices in the flow using PIV and described the turbulent motions in a turbulent boundary layer using these flow features. Furthermore, they explored the origin of large streamwise elongated structures through the collaborative motion of these vortices in the form of packets. These packet-like structures were also later introduced into the AEM [12]. These models rely on the chosen representative vortical structures, which are tailored in size, strength, inclination angle, wall-normal extension, and spatial distribution based on observations from numerical and experimental work. Due to the simplicity of the analytical models, they have a limited predictive capacity but provide insights into scaling behaviours even at high Reynolds numbers where simulations and experiments are impossible or at least hard to obtain. The flow fields predicted by the models are strongly dependent on the chosen eddies or vortex structures. For example, a notable difference between the models is that the hairpin model has long legs elongated in the streamwise direction which cause the well-known streaky flow pattern in the streamwise velocity component as outlined in Waleffe [17]. As the AEM does not have streamwise vortices it is expected that both models lead to fundamentally different statistical properties as outlined in Kähler *et al.* [18].

While single-point statistics can be well represented by a large number of different analytical models or eddy distributions [14,19,20], larger differences are observed in instantaneous spatial fields and multipoint statistics, likely due to the existence of other key structures in the flow and/or the overly simplified representative structures used. Recent works on the AEM have shown that some pertinent instantaneous spatial features of turbulent boundary layers can be reproduced by the representative structures employed in the AEM, e.g., uniform momentum zones or coherence of the spanwise velocity [21,22]. Despite these outcomes, further refinement of the structural composition in the AEM is necessary to improve its predictive capability of instantaneous spatial flow fields. To illustrate these shortcomings, Fig. 1 shows color contours of the streamwise velocity fluctuations u on a wall-parallel (xy) plane in the logarithmic region of a turbulent boundary layer. The left plane corresponds to an experimental flow field at $\mathrm{Re}_\tau = 4200$, and the right plane corresponds to a synthetic velocity field computed from a hierarchy of representative structures from the AEM model, to be detailed further in subsequent discussions (see also de Silva *et al.* [21], Woodcock and Marusic [23]). Despite the absolute values of the streamwise velocity fluctuations, u^+, being of the same order of magnitude and the flow features being qualitatively similar, some stark differences are visible. For example, the synthetic AEM flow-fields consist of regions of high (red) and low (blue) momentum that are always aligned in the streamwise or mean flow direction, which is consistent
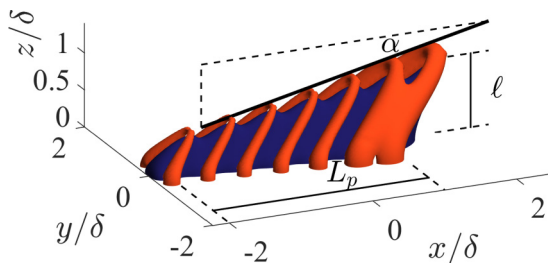
FIG. 2. Schematic of a typical representative Λ eddy used to generate the synthetic flow fields from the attached eddy model, adapted from de Silva *et al.* [21]. The blue region corresponds to the low-momentum region that forms beneath the packet of Λ eddies and the red region corresponds to a higher-speed region.

with how the representative structures are prescribed in the model [11]. The experimental flow field, however, is composed of elongated structures, which meander in the streamwise direction while convecting downstream. The meandering can be understood by considering the mutual interaction between the streak like flow motions and by assuming that the attached eddies or hairpin vortices have vortical legs of different strength and are not necessarily always symmetric. In this case, the stronger leg can bend the streak more than the weak leg. This asymmetry results in the meandering nature of the streaky motion. Alternatively, it can be assumed that the attached eddies or hairpin vortex legs have the same strength but the orientation of the structure is slightly angled to the flow direction. Recent works by Kevin *et al.* [24] quantified this behavior.

Accordingly, in the present work, we explore a subtle modification to the placement of eddies in the AEM model to introduce the meandering nature of these structures towards improving the spatial representation of the model. The paper is organized as follows: First, an overview of the synthetic AEM and experimental databases are provided. Thereafter, a comparison of the original AEM configuration with experimental data is presented. Based on our findings, the inclusion of meandering to the representative structures in the model is introduced in the subsequent section. Finally, the spanwise structural pattern is analyzed and discussed.

In this study, x, y, z correspond to the streamwise, spanwise, and wall-normal directions. U, V, W refer to the corresponding instantaneous velocities and u, v, w to the fluctuations. Mean velocities are denoted with an overbar and the superscript "+" corresponds to viscous units. For example, we use $l^+ = lU_\tau/\nu$ for length and $u^+ = u/U_\tau$ for velocity, where U_τ is the friction velocity and ν is the kinematic viscosity of the fluid.

II. ATTACHED-EDDY MODEL AND EXPERIMENTAL DATABASES

The flow fields discussed and analyzed in this paper are based on synthetic flow field databases computed from the AEM at $\mathrm{Re}_\tau = 3200$ and experimental databases captured in zero-pressure gradient flow conditions at $\mathrm{Re}_\tau \approx 4200$ and 8400.

A. Synthetic AEM flow fields

The synthetic flow fields from the AEM are computed based on a packet of Λ-eddies described in Marusic [12] and is depicted in Fig. 2. To date, this representative eddy has been shown to provide a good statistical representation of a turbulent boundary layer in the log-layer region [11]. A comprehensive mathematical description and instructions on how to generate the AEM flow fields can be found in Woodcock and Marusic [23] and de Silva *et al.* [21], respectively. To summarize, the vortex rods that constitute each Λ-eddy are assumed to contain a Gaussian distribution of vorticity about its core. To obtain a corresponding velocity field, Biot-Savart calculations are performed over all vortex rods present in a single representative eddy. This process is then repeated for each eddy within a packet and at different hierarchical length scales [11]. We note that the representative length

TABLE I. Flow and measurement parameters of the experimental databases.

Case	u_∞ m/s	Re_τ	$1/y^+$ μm	δ m	dt μs	Interrogation size pixel^2	Magnification	Vector spacing mm	Field of view m^2	Images
xy plane	12.4	4200	34.7	0.173	500	24×24	0.032	2.8	1.58×0.47	12 000
yz plane	31	8400	14.0	0.135	38	24×24	0.091	1	0.35×0.16	14 000

scales of eddies follow a geometric pattern, which can be exploited to minimise the computational cost due to the self-similarity of the structures at different hierarchical sizes. The assumption of self-similarity is supported by Sharma *et al.* [25]. Further, the spatial population density and domain size are held constant and selected such that the mean streamwise velocity profile in the logarithmic region satisfies the logarithmic-law constants [21].

B. Experimental databases

The experiments presented in this study are conducted in the Atmospheric Wind Tunnel Munich (AWM), which is a wind tunnel with a 22 m long test section at the Bundeswehr University Munich with a cross-sectional area of 1.85 m × 1.85 m, allowing flow velocities up to 40 m/s. Due to a long boundary layer development length of 10 m, a mean boundary layer thickness of $\delta_{99} \approx 0.145$ m is achieved at the measurement location. This allows experiments with Reynolds numbers up to $\mathrm{Re}_\tau = 13500$ under zero pressure gradient (ZPG) with high spatial resolution. Further details on the wind tunnel can be found in Reuther and Kähler [26].

For this study, two different datasets are employed which are captured using 2D-2C planar PIV and 2D-3C stereoscopic PIV. Four wall-parallel (*xy* planes) at wall distances $z/\delta =$ 0.06, 0.12, 0.23, and 0.45 were recorded through planar PIV measurements at $\mathrm{Re}_\tau = 4200$. Here, δ corresponds to the boundary layer thickness calculated based on a composite fit Chauhan *et al.* [27], which has been reported to be better suited when drawing comparisons to the synthetic AEM flow fields [21]. The SPIV measurement was made in a cross-flow (*yz* plane) configuration at $\mathrm{Re}_\tau = 8400$ to draw comparisons in wall-normal direction. For both datasets, the mean flow and higher-order statistics are in good agreement with existing zero pressure gradient boundary layer datasets [28–30].

For the PIV experiments, illumination was provided by a Spectra-Physics Quanta-Ray PIV Nd: YAG laser for the *xy*-plane measurement and an Innolas SpitLight 400 Compact Nd: YAG laser for the *yz*-plane measurement. The tracer particles were generated from Di-Ethyl-Hexyl-Sebacate (DEHS) with Laskin nozzle seeders, resulting in a mean tracer particle diameter of 1 μm [31]. To capture large coherent structures in their full spatial extent, three (planer PIV) and four (SPIV) PCO.edge 5.5 sCMOS cameras with a sensor size of 2560 × 2160 pixel were used in a multi-camera arrangement. This allowed us to capture the large fields of view specified in Table I with sufficient spatial resolution to resolve the smaller length scales in the flow. At least 12 000 statistically independent images were acquired for each measurement to ensure convergence of flow statistics [32]. PIV processing of the raw images was performed with DaVis software from LaVision using a multi-pass PIV algorithm with 50% interrogation window overlap. Thereafter, the individual vector fields of each camera were stitched together in Matlab to form a large flow field. More details on the PIV evaluation technique can be found in Raffel *et al.* [33]. A summary of the measurement details and parameters is given in Table I.

III. RESULTS AND DISCUSSION

A. Comparisons of the original AEM configuration with experimental data

The qualitative comparison between the synthetic AEM flow fields in Fig. 1 revealed some clear differences. To quantify these observations, statistical two-point correlations functions are computed
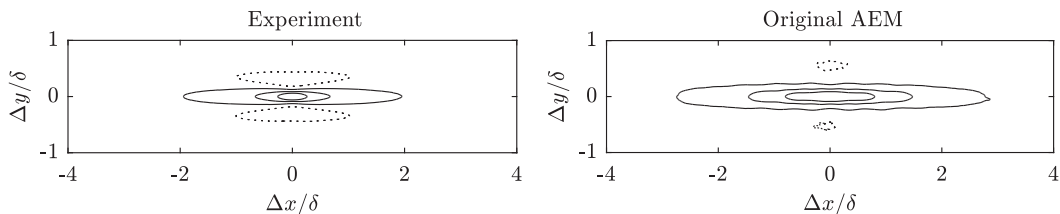
FIG. 3. Two-point correlation coefficient R_{uu} computed on a wall-parallel plane at $z/\delta = 0.06$. Left: Experimental database at $\mathrm{Re}_\tau = 4200$. Right: AEM synthetic flow fields at $\mathrm{Re}_\tau = 3200$. Solid lines represent positively correlated contour levels of $R_{uu} = 0.1$, 0.3, 0.5 and the dotted lines show negative correlation contour at $R_{uu} = -0.05$.

for both databases. The results are presented in Fig. 3, which shows the two-point correlation function R_{uu} for a wall-parallel plane at the same wall-height ($z/\delta = 0.06$), shown previously through instantaneous u contours in Fig. 1. A comparison of the positive regions of R_{uu}, reveals that results from the synthetic AEM flow fields are wider in the spanwise direction and more elongated in the streamwise direction. This can be explained through assumptions in the model. Specifically, the elongated correlations in x are caused by streamwise aligned eddies within a packet, which induces fluid with relatively similar velocity in their core region (blue region in Fig. 2), while between packets high momentum flow regions are generated dependent on the spanwise separation. Furthermore, the placement of eddies is such that they are all aligned to the flow direction, while the experimental data exhibits that these regions of coherence appear to meander and are not necessarily always aligned to the direction of the flow [24]. These spatial differences are inherently associated with the dynamics of the eddies in a turbulent boundary layer and their spatial organization, which we aim to address toward better representing these flow structures instantaneously in the attached eddy model.

B. The influence of meandering structures in the attached eddy model

From its conception, the placement of representative eddies in the AEM is considered to be aligned with the direction of the flow [10,12]. Instead, based on the preceding discussions, to include a degree of meandering in the flow structures, we consider that the eddies are allowed to be angled to the direction of the flow. Specifically, we introduce a parameter θ that corresponds to the angle between the major axis of the representative Λ- eddies and the flow direction, illustrated in Fig. 4.
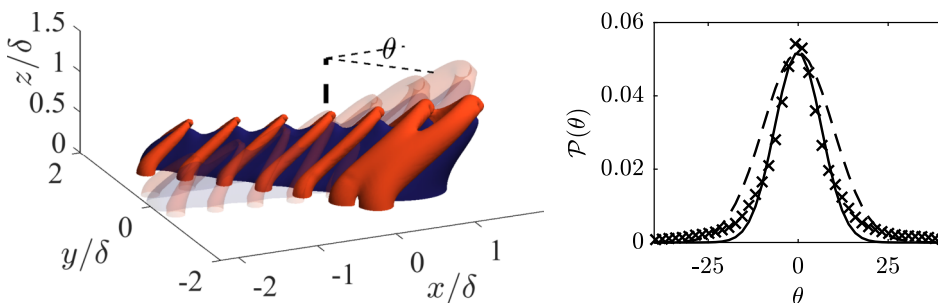

FIG. 4. Left: Schematic illustrating the meandering angle θ which is imposed on the representative AEM structures. Right: Probability distribution of θ, where $\theta = 0$ corresponds to the streamwise direction x. $\times$ symbols: Distribution based on results reported by Kevin *et al.* [24]. Solid line (-): Gaussian fit of the experimental data with similar standard deviation σ. Dashed line (- -): Gaussian fit of the experimental data with increased standard deviation 1.5σ.
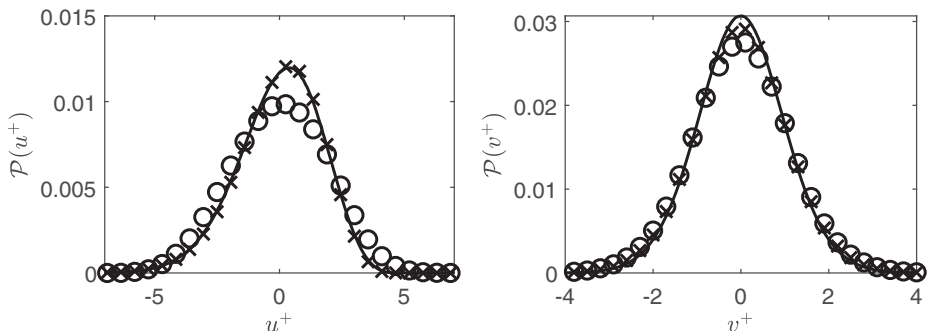
FIG. 5. Probability distribution of the streamwise u^+ (left) and spanwise v^+ (right) fluctuations in a wall-parallel plane at $z/\delta = 0.07$. Black line (-) corresponds to the original AEM. × symbols correspond to the modified AEM. ○ symbols represent the experimental data at $Re_\tau = 4200$.

To introduce this modified AEM configuration the distribution of θ is based on the results reported by Kevin *et al.* [24] for coherent regions of streamwise velocity in turbulent boundary layers.

A PDF of the imposed distribution of θ is reproduced in Fig. 4. In addition, results from a Gaussian fit to the same distribution (solid line) is included along with a second distribution with an increased standard deviation (dashed line). These distributions will be employed in the subsequent discussions to assess the influence of the distribution of θ. It should be noted, the proposed methodology to introducing meandering of the representative structures in the AEM without any modification to the eddy shape, minimises any impact on the mean-flow statistics which have been reported to be in good agreement to experimental data [21,23]. To quantify the influence of the meandering on the flow velocities, the probability distribution of the streamwise u^+ and spanwise v^+ fluctuations from the modified and original synthetic AEM flow fields are compared to the experimental data in Fig. 5. The results reveal minimal impact on u while v appears to better represent the experimental data.

Figure 6 shows color contours of streamwise velocity fluctuations of the original AEM configuration (top), the modified AEM configuration (center), and the reference experimental data (bottom).
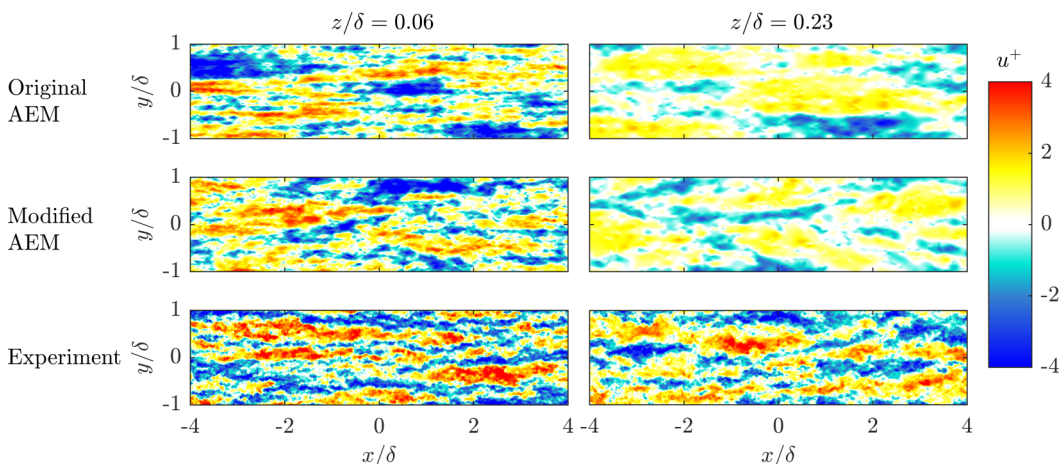

FIG. 6. Comparison of instantaneous streamwise velocity fluctuations fields u^+ based on the original AEM configuration (top), the modified AEM configuration (middle) and experiments (bottom). Left column: Wall distance $z/\delta = 0.06$. Right column: Wall distance $z/\delta = 0.23$.
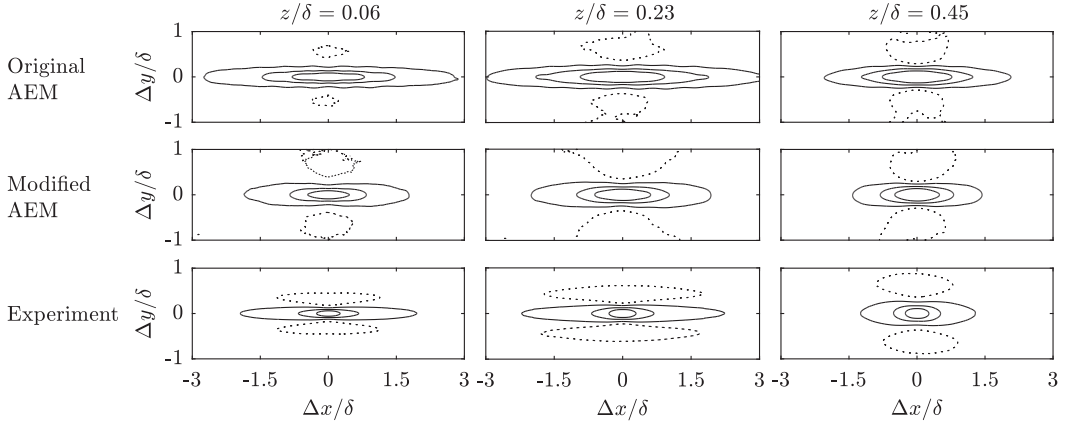
FIG. 7. Two-point correlation coefficient R_{uu} for wall-parallel planes at $z/\delta = 0.06$ (left column), $z/\delta = 0.23$ (middle column), and $z/\delta = 0.45$ (right column). Top row: original AEM configuration at $Re_\tau = 3200$. Middle row: modified AEM configuration at $Re_\tau = 3200$. Bottom row: Experiment at $Re_\tau = 4200$. Solid lines represent contour levels of $R_{uu} = 0.1$, 0.3, 0.5 and the dotted lines correspond to a contour level of $R_{uu} = -0.05$.

Results are presented at two wall-normal heights of $z/\delta \approx 0.06$ and $z/\delta \approx 0.23$. Qualitatively, the results reveal that the large-scale streamwise coherence in the modified AEM synthetic flow fields is a closer match to the experiments and exhibits meandering characteristics, similar to those from the experimental databases.

To further quantify this behavior, the modified AEM configuration flow fields are analyzed employing two-point correlations. The resulting R_{uu} is shown in Fig. 7 at $z/\delta = 0.06$, $z/\delta = 0.23$ and $z/\delta = 0.45$, which reveals that the streamwise extent of the positively correlated region of R_{uu} from the modified AEM configuration flow fields is better matched to the experiments at all wall-normal heights considered. A closer inspection of the positive correlation contours from the original AEM flow fields reveals a wavy shape due to the fixed spacing between the Λ-eddies in a packet and the forced streamwise alignment of all eddies, while the experimental results exhibit a narrow neck flanking the correlation point (see also Ref. [34]). This behavior from the experiments also appears to be better reproduced from the modified AEM flow fields due to the asymmetry introduced due to the meandering imposed on the eddies.

In contrast to the streamwise extent, the width of the positively correlated regions in the spanwise direction is larger in the AEM flow fields. However, this is likely due to exact physical dimensions of the representative eddy shape, which has been chosen here to follow recent works [21,23]. These works have shown that flow statistics computed employing this eddy-shape provides a logarithmic-law constant and Reynolds stresses that is in good agreement to experiments, therefore, we believe the chosen representative eddy forms a good baseline for the present study. It must be stressed that the present contribution is to introduce meandering to the representative eddies in the AEM towards better representing the instantaneous structures in a turbulent boundary layer.

To quantify this behavior further, a length scale L and width scale W are calculated from the wall-parallel two-point correlation functions using a threshold of $R_{uu} = 0.15$ and is presented in Fig. 8. As expected, the length L of the modified AEM configuration is reduced compared to the original configuration due to the meandering and appears to better match the experimental data. To study the influence and sensitivity of the meandering angle distribution, three different distributions, as shown in Fig. 4, are tested. The results reveal that the general trend is consistent for the angle distributions. Specifically, only small differences in the length L is observed between the original distribution from Kevin *et al.* [24] and a Gaussian fit, while a fit with a 50% increase in standard deviation leads to increased meandering and therefore a slightly shorter structure length.
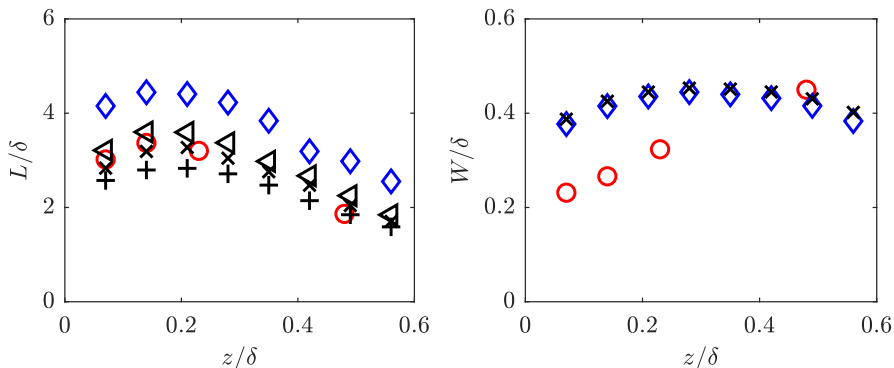
FIG. 8. Comparison of the original AEM configuration ($\diamond$ symbols), the modified AEM configuration ($\times$ symbols), and the experimental data at $\mathrm{Re}_\tau = 4200$ ($\circ$). We note, $\times$ symbols correspond results computed based on the angle distribution $P(\theta)$ form Kevin *et al.* [24], while the $\triangleleft$ and $+$ symbols correspond to results computed from Gaussian distributions fitted to $P(\theta)$ with a standard deviation of $1\,\sigma$ and $1.5\,\sigma$, respectively. Left: Streamwise length L. Right: Spanwise width W. Length and width are calculated from the wall-parallel two-point correlations using a threshold of $R_{uu} = 0.15$.

In addition to the streamwise length L, the spanwise width W is analyzed and plotted in Fig. 8. The influence of the meandering on the width is small. In contrast to the length L, the general scaling trend is not well reproduced by the AEM. This trend is directly related to the chosen eddy shape and size and can therefore be improved by further refinement of the representative eddy employed in the AEM. Furthermore, as all eddies in the AEM are wall-coherent or "attached" to the wall inclusive of the largest eddies that extend to the outer edge of the boundary layer, the resulting width, W, from the two-point correlations is likely to be overestimated closer to the wall.

C. Cross-plane results

To draw further comparisons on the spatial coherence in the synthetic flow fields from the AEM, the cross-stream yz plane is explored. To this end, Fig. 9 shows a comparison of instantaneous flow fields in the yz plane from the experimental and synthetic AEM datasets. Qualitatively, a comparison between the original and modified AEM flow fields reveals that the meandering of the representative structures introduced to the model induces an asymmetry/tilt on this plane, which is closer to the behavior observed from the experiments (see also Jiménez [1], Kevin *et al.* [24]). To quantify this
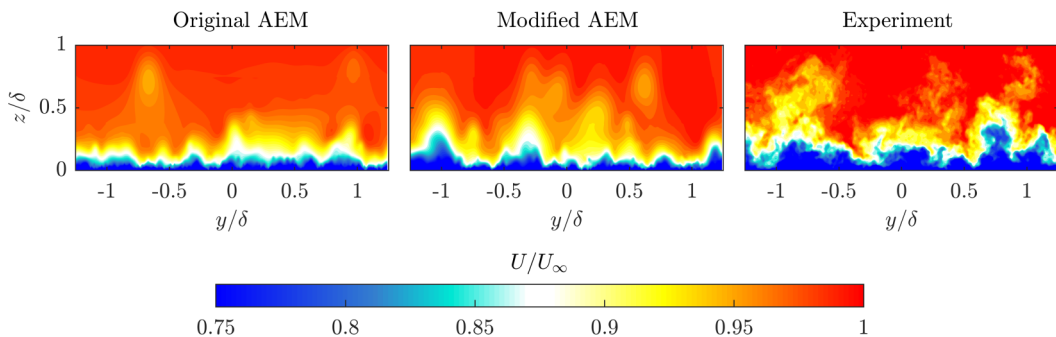

FIG. 9. Instantaneous color contours of streamwise velocity U/U_∞ on a cross-stream yz-plane. Left: Generated flow field based on the original AEM. Middle: Flow fields based on the modified AEM configuration. Right: Experimental data.
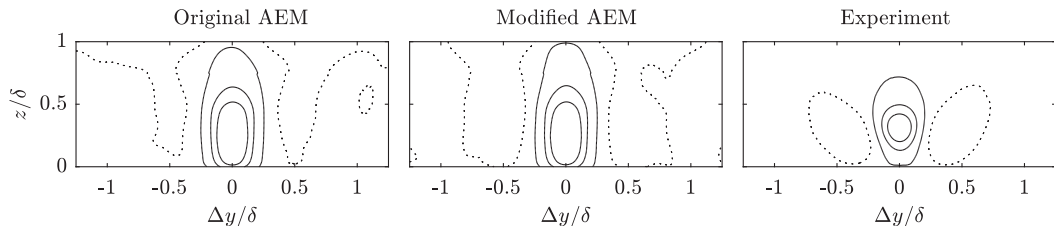
FIG. 10. Two-point correlation coefficient R_{uu} for a correlation point at $z/\delta = 0.24$. Left: Original AEM configuration. Middle: Modified AEM configuration. Right: Experimental data. Solid lines represent positive correlated areas, dotted lines negative correlation.

observation, R_{uu} computed in the yz plane is presented in Fig. 10 for a correlation point at a wall distance of $z/\delta = 0.24$. The results from all the datasets exhibit positively correlated regions flanked by regions of negative correlation, highlighting the similarity between the model and experiments. However, results from the AEM model are dominated by the largest representative eddy with a height of δ. Specifically, the AEM exhibits that the positively correlated regions of R_{uu} near the wall are wider and become narrower with increasing z. This concurs with the Λ shaped eddy employed to generate the synthetic flow fields, which has a triangular form in the yz plane. For the experimental data, the opposite is the case with a narrower region close to the wall, which is primarily due to all the structures in a turbulent boundary layer not being wall-coherent as defined by the AEM. Therefore, future refinements to the AEM are likely to involve the inclusion of wall-incoherent flow features, particularly in the wake region (see also Hwang and Sung [35]).

Overall, the modified AEM configuration improved the spatial representation of the streamwise velocity component U of the synthetic flow fields by the AEM in the logarithmic region. Absolute deviations in width or height are parameters which themselves depend on the eddy shape used and the chosen eddy size. Furthermore, the two-point correlation provides a measure of the spatial scales, e.g., the width, based on a chosen threshold. One should also keep in mind that small-scale turbulence influences the magnitude of the positive correlation on average and is not present in the AEM as we move away from the wall. Additionally, the PIV fields are inherently spatially low pass filtered by the measurement technique. Specifically, the spatial resolution of a PIV measurement is directly dependent on the final interrogation window size or double the vector spacing, which equals 160 viscous units for wall-parallel measurements and 140 viscous units for the cross-stream plane measurements.

D. Analysis of the spanwise velocity component

In the preceding discussions, the streamwise velocity fluctuations u is examined. Recent works by de Silva *et al.* [22], Sillero [36], also highlighted particular patterns in the large-scale spanwise coherence of the spanwise velocity within turbulent boundary layers. In a similar fashion, Fig. 11 shows the instantaneous spanwise velocity fluctuations v^+ between the synthetic AEM flow fields and the experiments on wall-parallel planes at $z/\delta = 0.06$ and $z/\delta = 0.23$. The results show a strong periodicity in flow direction for the original AEM configuration (top), while the modified AEM configuration (centre) and the experiments (bottom) exhibit better agreement. We note, similar to the flow fields of u^+ in Fig. 6, the AEM flow fields appear less turbulent, especially in the plane further away from the wall at $z/\delta = 0.23$, due to the absence of small-scale turbulence in the AEM with increasing z.

To quantify the spatial features in the v coherence further, Fig. 12, shows R_{vv} computed on xy planes at $z/\delta = 0.06$ (left column), $z/\delta = 0.23$ (middle column) and $z/\delta = 0.45$ (right column). The results reveal that the spatial extent of the coherence for v is less compared to u, which is in line with previous observation in literature [22,36,37]. We note, a strong periodicity in R_{vv} is observed
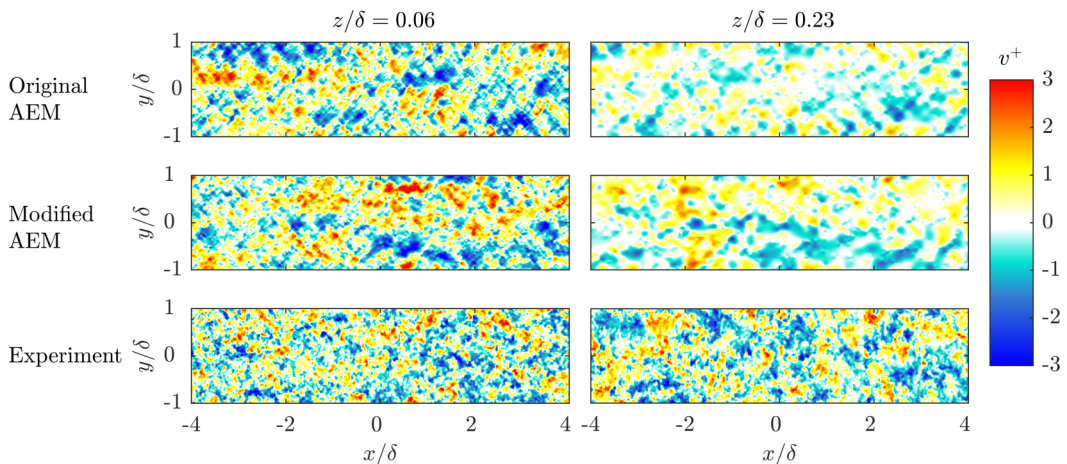
FIG. 11. A comparison of instantaneous spanwise velocity fluctuations v^+ based on the original AEM configuration (top), the modified AEM configuration (middle) and experiments (bottom). Left column: Wall distance $z/\delta = 0.06$. Right column: Wall distance $z/\delta = 0.23$.

from the original AEM configuration flow fields with a wavelength equal to eddy spacing within the representative packet eddy employed. This artificial periodicity is significantly reduced by the meandering introduced in the modified AEM configuration, leading to an improved agreement to the experiments. Further, the spatial extent of the v coherence also appears to be better matched between the modified AEM configuration and the experiments.

The contours of R_{vv} exhibit a squarish shape from all datasets similar to that reported by de Silva *et al.* [22], Sillero [36]. Inspired by these observations on the xy plane, contours of R_{vv} from the yz plane are shown in Fig. 13 for the modified AEM configuration and experiments. Results are computed at $z/\delta = 0.2$ (black) and $z/\delta = 0.8$ (red). To emphasize the influence of v, the fields are conditioned on $v < -0.5\sigma_v$ and $v > 0.5\sigma_v$, where σ_v corresponds to the standard deviation of v. At
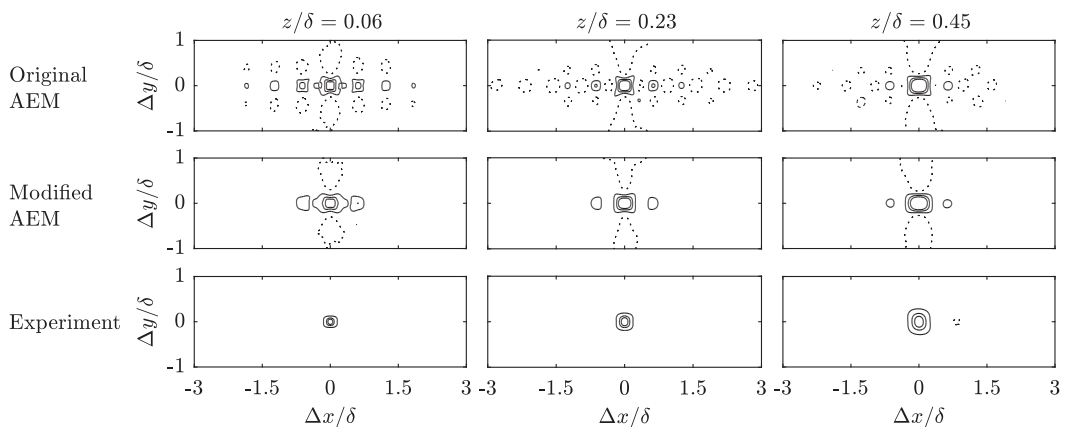

FIG. 12. Two-point correlation coefficient R_{vv} for the spanwise velocity fluctuations computed on wall-parallel planes at $z/\delta = 0.06$ (left column), $z/\delta = 0.23$ (middle column) and $z/\delta = 0.45$ (right column). Top row: Original AEM configuration at $\mathrm{Re}_\tau = 3200$. Middle row: Modified AEM configuration at $\mathrm{Re}_\tau = 3200$. Bottom row: Experiment at $\mathrm{Re}_\tau = 4200$. Solid lines represent contour levels of $R_{vv} = 0.15,\ 0.3,\ 0.45$ and the dotted line corresponds to a contour level of $R_{vv} = -0.075$.
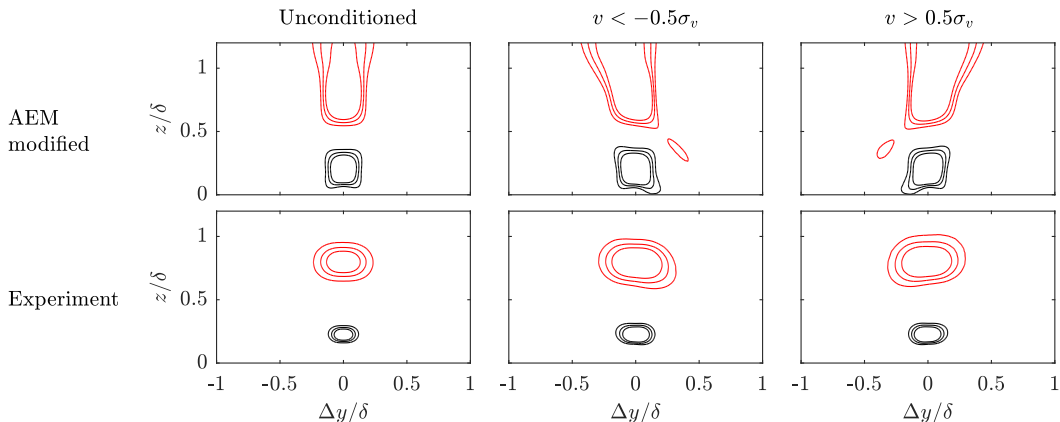
FIG. 13. Conditioned two-point correlation coefficient R_{vv} for a correlation point at $z/\delta = 0.2$ (black) and $z/\delta = 0.8$ (red). Top row: modified AEM configuration. Bottom row: Experimental data. Solid lines represent contour levels at $R_{vv} = 0.3, 0.4, 0.5$. The left column represents all data, middle column conditioned in the correlation point on $v < -0.5\sigma_v$, right column conditioned on $v > 0.5\sigma_v$.

$z/\delta = 0.8$, the conditional results reveal a strong diagonal orientation dependent on the sign of v in both the experiments and the modified AEM flow fields similar to the findings of de Silva *et al.* [22], Sillero [36] on the *xy* plane. These findings also agree with the conceptual "leaning" behavior discussed in Ref. [24]. Closer to the wall at $z/\delta = 0.2$ all databases reveal a squarish/elliptical shape; however, if R_{vv} is conditioned on the direction of v, then the same diagonal orientation is observed, albeit less pronounced, particularity in the experiments. Further, the coherence from the AEM fields exhibits a larger spatial extent with increasing z as the eddy size increases with the wall distance. This effect is directly visible when comparing the correlation results at $z/\delta = 0.2$ and $z/\delta = 0.8$. To improve the spatial representation, it is, therefore, necessary to decorrelate large eddies from the wall. In the experimental data, this effect is inherently present, because all turbulent structures are not "attached" to the wall, which leads to a decorrelation in the near-wall region.

IV. SUMMARY AND CONCLUSIONS

A comparison between synthetic flow fields based on the attached eddy model (AEM) and experimental data is presented to examine the predictive capabilities of spatial features in turbulent boundary layers from the model. To this end, the streamwise velocity and spanwise velocity components are analyzed qualitatively and quantitatively on wall-parallel and cross-stream planes. Our results reveal that the resulting spatial coherence of the AEM synthetic flow fields is too strong and do not reproduce the meandering behavior of flow features to the direction of flow.

Based on these observations, a modified AEM configuration is introduced to improve the spatial representation which incorporates the meandering of large-scale structures to the flow direction. Our results confirm that the spatial representation of the instantaneous flow features is improved through this inclusion by reducing periodic effects and improving the estimation of spatial coherence. Further, inspired by recent works on the spanwise large-scale coherence on the wall-parallel plane we report the presence of a similar preferential diagonal orientation of the spanwise coherence dependent on the sign of the spanwise velocity on the cross-stream plane, which is present in the experiments and is also captured by the modified AEM flow fields.

Although the modified AEM and the experimental data shows improved similarity, the multipoint statistics are still observed to differ in the cross-plane for two main reasons. First, the AEM does not account for intermittency effects, which leads to increased correlation in the wake region. Second, the near-wall structures are different from logarithmic-layer structures in a turbulent boundary layer

flow and the model does not account for flow structures that do not extend to the wall. Hence, the correlation is increased down to the wall. Further, we note, the AEM is a statistically based model that does not directly account for the dynamic aspects of the flow motion, which include the generation, development and decay of the eddies, nor their formation into packets. However, the model is well suited to describing the kinematic state of the boundary layer and future work towards further improvements are warranted.

[1] J. Jiménez, Coherent structures in wall-bounded turbulence, J. Fluid Mech. **842**, 1 (2018).

[2] J. M. Wallace, Highlights from 50 years of turbulent boundary layer research, J. Turbul. **13**, N53 (2012).

[3] B. J. Balakumar and R. J. Adrian, Large-and very-large-scale motions in channel and boundary-layer flows, Philos. Trans. R. Soc., A **365**, 665 (2007).

[4] N. Hutchins, K. Chauhan, I. Marusic, J. P. Monty, and J. Klewicki, Towards reconciling the large-scale structure of turbulent boundary layers in the atmosphere and laboratory, Bound.-Lay. Meteorol. **145**, 273 (2012).

[5] S. K. Robinson, Coherent motions in the turbulent boundary layer, Annu. Rev. Fluid Mech. **23**, 601 (1991).

[6] T. Theodorsen, Mechanism of turbulence, in *Proceedings of the Midwestern Conference on Fluid Mechanics* (University of Minnesota, 1952), pp. 1–18.

[7] C. Smith, A synthesized model of the near-wall behavior in turbulent boundary layers., Tech. Rep. (Lehigh University Bethlehem Pa, Department of Mechanical Engineering and Mechanics, 1984).

[8] A. A. Townsend, *The Structure of Turbulent Shear Flow* (Cambridge University Press, Cambridge, UK, 1956).

[9] R. J. Adrian, C. D. Meinhart, and C. D. Tomkins, Vortex organization in the outer region of the turbulent boundary layer, J. Fluid Mech. **422**, 1 (2000).

[10] A. E. Perry, S. Henbest, and M. Chong, A theoretical and experimental study of wall turbulence, J. Fluid Mech. **165**, 163 (1986).

[11] I. Marusic and A. E. Perry, A wall-wake model for the turbulence structure of boundary layers. Part 2. Further experimental support, J. Fluid Mech. **298**, 389 (1995).

[12] I. Marusic, On the role of large-scale structures in wall turbulence, Phys. Fluids **13**, 735 (2001).

[13] T. B. Nickels, I. Marusic, S. Hafez, N. Hutchins, and M. S. Chong, Some predictions of the attached eddy model for a high Reynolds number boundary layer, Philos. Trans. R. Soc., A **365**, 807 (2007).

[14] I. Marusic and J. P. Monty, Attached eddy model of wall turbulence, Annu. Rev. Fluid Mech. **51**, 49 (2019).

[15] S. J. Kline, W. C. Reynolds, F. Schraub, and P. Runstadler, The structure of turbulent boundary layers, J. Fluid Mech. **30**, 741 (1967).

[16] M. Head and P. Bandyopadhyay, New aspects of turbulent boundary-layer structure, J. Fluid Mech. **107**, 297 (1981).

[17] F. Waleffe, Three-Dimensional Coherent States in Plane Shear Flows, Phys. Rev. Lett. **81**, 4140 (1998).

[18] C. Kähler, R. Adrian, and C. Willert, Turbulent boundary layer investigations with conventional and stereoscopic PIV, in *Proceedings of the 9th International Symposium on Application of Laser Technology to Fluid Mechanics, Lisbon Portugal*, Vol. 11 (1998), pp. 13–16.

[19] M. Pamiès, P. Weiss, E. Garnier, S. Deck, and P. Sagaut, Generation of synthetic turbulent inflow data for large eddy simulation of spatially evolving wall-bounded flows, Phys. Fluids **21**, 045103 (2009).

[20] Q. Zhang, W. Schröder, and M. Meinke, A zonal rans-les method to determine the flow over a high-lift configuration, Comput. Fluids **39**, 1241 (2010).

[21] C. M. de Silva, J. D. Woodcock, N. Hutchins, and I. Marusic, Influence of spatial exclusion on the statistical behavior of attached eddies, Phys. Rev. Fluids **1**, 022401 (2016).

[22] C. de Silva, K. Kevin, R. Baidya, N. Hutchins, and I. Marusic, Large coherence of spanwise velocity in turbulent boundary layers, J. Fluid Mech. **847**, 161 (2018).

[23] J. Woodcock and I. Marusic, The statistical behavior of attached eddies, Phys. Fluids **27**, 015104 (2015).

[24] K. Kevin, J. P. Monty, and N. Hutchins, The meandering behavior of large-scale structures in turbulent boundary layers, J. Fluid Mech. **865**, R1 (2019).

[25] A. Sharma, R. Moarref, and B. McKeon, Scaling and interaction of self-similar modes in models of high Reynolds number wall turbulence, Philos. Trans. R. Soc., A **375**, 20160089 (2017).

[26] N. Reuther and C. Kähler, Evaluation of large-scale turbulent/nonturbulent interface detection methods for wall-bounded flows, Exp. Fluids **59**, 121 (2018).

[27] K. A. Chauhan, P. A. Monkewitz, and H. M. Nagib, Criteria for assessing experiments in zero pressure gradient boundary layers, Fluid Dyn. Res. **41**, 021404 (2007).

[28] M. Novara, D. Schanz, R. Geisler, S. Gesemann, C. Voss, and A. Schröder, Multi-exposed recordings for 3D Lagrangian particle tracking with multi-pulse shake-the-box, Exp. Fluids **60**, 44 (2019).

[29] T. Knopp, M. Novara, D. Schanz, E. Schülein, A. Schröder, N. Reuther, and C. J. Kähler, A new experiment of a turbulent boundary layer flow at adverse pressure gradient for validation and improvement of RANS turbulence models, in *New Results in Numerical and Experimental Fluid Mechanics XI* (Springer, Berlin, 2018), pp. 85–94.

[30] T. Knopp, M. Novara, D. Schanz, R. Geisler, F. Philipp, M. Schroll, C. Willert, and A. Schröder, Modification of the SSG/LRR-ω RSM for turbulent boundary layers at adverse pressure gradient with separation using the new DLR VicToria experiment, in *Symposium der Deutsche Gesellschaft für Luft-und Raumfahrt* (Springer, Berlin, 2018), pp. 80–89.

[31] C. Kähler, B. Sammler, and J. Kompenhans, Generation and control of tracer particles for optical flow investigations in air, in *Particle Image Velocimetry: Recent Improvements* (Springer, Berlin, 2004), pp. 417–426.

[32] C. Kähler, S. Scharnowski, and C. Cierpka, Highly resolved experimental results of the separated flow in a channel with streamwise periodic constrictions, J. Fluid Mech. **796**, 257 (2016).

[33] M. Raffel, C. E. Willert, F. Scarano, C. J. Kähler, S. T. Wereley, and J. Kompenhans, *Particle Image Velocimetry: A Practical Guide* (Springer, Berlin, 2018).

[34] N. Hutchins and I. Marusic, Evidence of very long meandering features in the logarithmic region of turbulent boundary layers, J. Fluid Mech. **579**, 1 (2007).

[35] J. Hwang and H. J. Sung, Wall-attached structures of velocity fluctuations in a turbulent boundary layer, J. Fluid Mech. **856**, 958 (2018).

[36] J. Sillero, High Reynolds number turbulent boundary layers, Ph.D. thesis, Universidad Politénica de Madrid, 2014.

[37] N. Hutchins, W. T. Hambleton, and I. Marusic, Inclined cross-stream stereo particle image velocimetry measurements in turbulent boundary layers, J. Fluid Mech. **541**, 21 (2005).